# Piezo1 activates non-canonical EGFR endocytosis and signaling

Carlos Pardo-Pastor [a, *] and Jody Rosenblatt [a, b *]

ORCID: 0000-0003-4083-0511 (C.P.-P.), 0000-0001-9460-5868 (J.R.)

[a] Randall Centre for Cell & Molecular Biophysics, New Hunt's House, School of Basic & Medical Sciences; and [b] School of Cancer & Pharmaceutical Sciences; Faculty of Life Sciences & Medicine, King's College London, SE1 1UL London, United Kingdom

*Correspondence to: carlos.pardo-pastor@kcl.ac.uk or jody.rosenblatt@kcl.ac.uk

Classification: Biological Sciences-Cell Biology

Keywords: Piezo1, EGFR, Epithelia, Signaling, Proliferation, Migration, Extrusion

# Abstract

EGFR-ERK signaling controls cell cycle progression during development, homeostasis, and disease. Both the soluble extracellular ligand, EGF, and mechanical inputs like matrix stiffness, cell adhesion, or stretch can activate EGFR-ERK signaling. However, the molecules transducing mechanical forces into EGFR signaling remain unidentified. We previously found that stretch promotes mitosis by mechanically activating the ion channel Piezo1 to trigger ERK signaling. Here, we show that Piezo1 provides the missing link to mechanical EGFR-ERK activation. Both EGF or the synthetic Piezo1 agonist Yoda1 triggered EGFR internalization and ERK activation, established markers of EGFR signaling. However, while EGF stimulation requires canonical EGFR tyrosine autophosphorylation, activation by Piezo1 requires non-canonical serine EGFR phosphorylation by a Src-p38 kinase axis. Additionally, Yoda1 stimulation of Piezo1 promoted cell cycle re-entry and proliferation via long-term nuclear accumulation of ERK, AP-1 (FOS and JUN), and YAP, typical of regenerative and malignant signaling. Our results suggest two modes of EGFR signaling: basal EGF-dependent signaling, requiring tyrosine autophosphorylation, and mechanically activated EGFR signaling, that results in sustained proliferation, critical to repair and regeneration, and cancer growth.


# Significance statement

Epidermal Growth Factor Receptor (EGFR) controls complex functions like cell cycle progression and migration during both homeostasis and disease. Typically, EGF activation of EGFR controls homeostatic functions via tyrosine autophosphorylation and endocytosis. However, mechanical forces can activate EGFR during regeneration and metaplasia. Here, we show that the stretch-activated ion channel Piezo1 provides the missing link for mechanical EGFR-ERK activation via non-canonical serine EGFR phosphorylation by a Src-p38 kinase axis. Piezo1 activation caused nuclear accumulation of the kinase ERK, proto-oncogenes FOS and JUN, and the transcriptional regulator YAP and cell cycle re-entry. Discovery of Piezo1-dependent EGFR activation, therefore, could provide a promising therapeutic cancer target.

# Main text

## Introduction

The plasma membrane of animal cells forms interfaces between cells, the underlying matrix, and the cell exterior. It also contains different transmembrane proteins—ion channels, integrins, Receptor Tyrosine Kinases (RTKs), or G Protein Coupled Receptors (GPCRs)—that can detect extracellular signals with variable specificity. The nature of the stimulus and the combination of detector and effector mechanisms determine differential downstream cellular responses (1, 2). One stimulus can activate more than one receptor and some receptors transactivate others (3–7). Complex cell functions like cell cycle regulation or migration arise from integrating agonist and antagonist inputs that signal via different receptors and effectors (1, 2).

Mechanical regulation of cell proliferation, differentiation, and migration was originally described decades ago (8–10), but only recently have molecules that integrate mechanics and signaling come to light. The mechanosensitive Piezo ion channels and YAP/TAZ transcriptional regulators are the most noteworthy in this integration (11–14). Human Piezo1 and 2 are mechanically activated cation channels, abundant in a wide variety of tissues and cell types (11), that mediate extracellular calcium influx in response to cell confinement (15), stretch (16), shear stress (17), or matrix stiffness (18, 19). Piezo-dependent calcium entry is critical for development, regeneration, and cancer through its roles in cell migration (15, 18), matrix remodeling (18, 20), mitotic cytokinesis (16), or stiffness-induced nuclear translocation of YAP (18, 19). Our group found that Piezo1 promotes epithelial cell extrusion in response to crowding (21) and rapid cell division ($G_2$/M transition) in response to stretch (22). Moreover, stretch also promotes cell exit from quiescence ($G_0$/$G_1$ transition) and DNA synthesis ($G_1$/S transition) (23), both of which are prevented by Piezo1 knockdown (24). These studies strengthen a general role for mechanical forces and Piezo1 as master regulators of the cell cycle.

Soluble growth factors also regulate cell function via membrane receptors. Epidermal Growth Factor Receptor (EGFR) is a widely expressed RTK that autophosphorylates its C-terminal cytoplasmic tyrosine residues after binding extracellular soluble ligands (1, 2, 4, 5, 25, 26). These modified residues act as docking sites for adaptor proteins containing phosphotyrosine (pY)-binding SH2 domains, such as SHC and GRB2. Effector proteins (GEFs-Ras-MAPK, PKB/AKT, PLC, PI3K modules) bind pY-bound adaptors, and their specific combination and phosphorylation by EGFR triggers downstream signaling pathways such as RAS-MAPK that impact cell migration, the cell cycle (cell division, quiescence and DNA synthesis), and tumor malignancy (1–3, 5, 25, 27–34).

Mechanical signals such as cell stretch (28, 29), apicobasal compression (7), matrix-cell adhesion and cell spreading (3, 31, 35, 36), or matrix stiffness (25, 30, 33) activate EGFR. Moreover, matrix stiffness also promotes EGFR expression, clustering, and EGF binding (25). Therefore, mechanical signals also modulate canonical EGFR signaling in response to soluble ligands. However, the identity of the molecules transducing mechanical forces into EGFR-activating signals remains unknown. Notably, calcium increases activate phosphorylation and downstream signaling of several RTKs (5). Additionally, we previously found that loss or inhibition of Piezo1 prevents stretch-activation of the MAPK ERK (22), a target of EGFR, suggesting that Piezo1 may activate EGFR signaling.

## Results

### Synthetic Piezo1 activation triggers EGFR endocytosis

To directly activate Piezo1 without triggering other mechanosensitive pathways, we used the synthetic Piezo1 agonist Yoda1 (37) and monitored internalization of EGFR phosphorylated on tyrosine 1173 (pY1173-EGFR), an indicator of active EGFR signaling (25, 35, 38, 39). Here, we use HeLa cells because they express Piezo1 endogenously and are widely used for EGFR studies (26, 39–42)(42). Serum-starved HeLa cells treated with 10 μM Yoda1 or 10 ng/mL EGF redistributed pY1173-EGFR from the cell periphery to intracellular puncta that colocalize with the early endosome marker EEA1 within 15 minutes (Fig.1A-D). siRNA-mediated Piezo1 knockdown (siPiezo1) suppressed calcium signaling (Fig.S1A-C) and pY1173-EGFR internalization in response to Yoda1 but did not significatively affect responses to EGF (Fig.S1D, E). These results show that Yoda1 triggers Piezo1-dependent EGFR endocytosis into early endosomes.

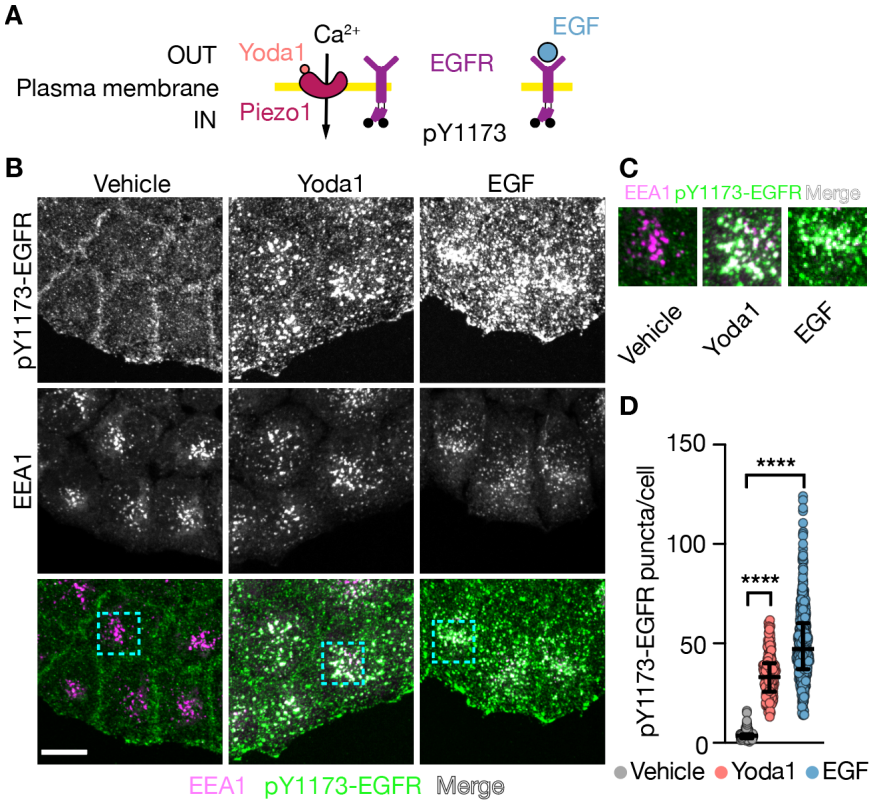


**Figure 1. EGFR endocytosis in response to the Piezo1 agonist Yoda1.**

(A) Schematic of the experimental set-up. (B) Representative maximum intensity projections of pY1173-EGFR and EEA1 co-stainings in HeLa cells treated for 15min with vehicle, 10μM Yoda1 or 10ng/mL EGF. (C) Inserts from regions indicated in B. (D) Counts of pY1173-EGFR puncta per cell. Each symbol represents a cell. Vehicle: 389, Yoda1: 454, EGF: 925, 4 experiments. Scale bar = 20μm. Error bars = median±interquartile range. **** $p < 0.0001$ in one-way ANOVA followed by Kruskal-Wallis post-hoc test with Dunn's correction for multiple comparisons.

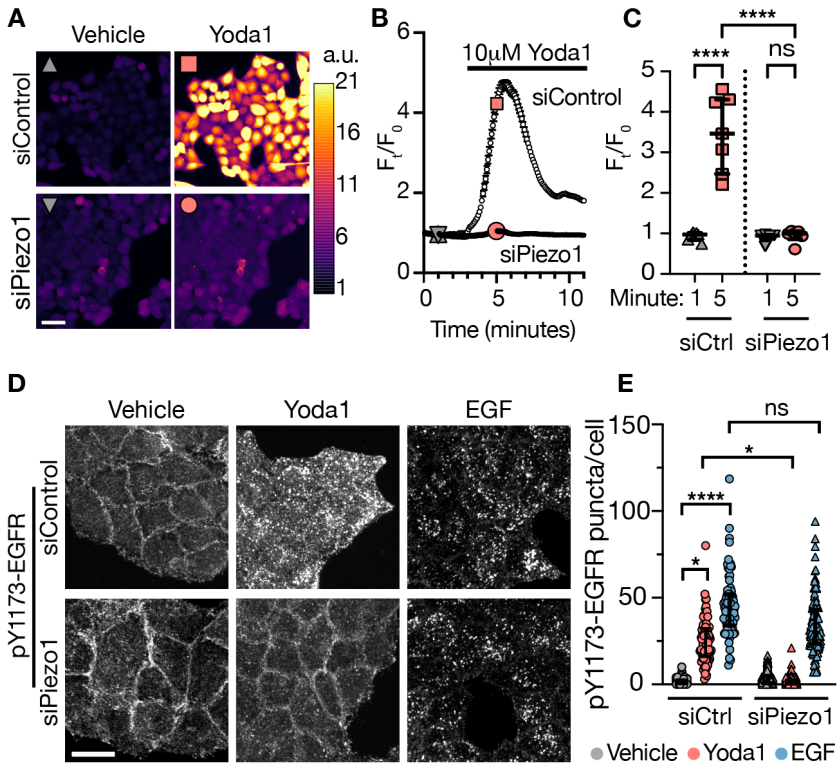


**Figure S1. Piezo1 knockdown suppresses responses to Yoda1.**

(A, B, C) Representative pseudo-coloured micrographs (A), mean traces (B), and summary statistics (C) of fluorescence intensity in siRNA-transfected HeLa cells loaded with the $Ca^{2+}$ indicator Calbryte520AM before and after 10μM Yoda1 treatment. siCtrl: 673 cells, 7 independent experiments, 3 transfections; siPiezo1: 1007 cells, 6 independent experiments, 3 transfections. (D) Representative maximum intensity projections of pY1173-EGFR stainings in control and Piezo1 KD HeLa cells HeLa cells treated with vehicle, 10μM Yoda1, or 10ng/mL EGF. (E) Counts of pY1173-EGFR puncta per cell. Each symbol represents a cell. siCtrl (431 Vehicle, 231 Yoda1, 221 EGF), siPiezo1 (611 Vehicle, 702 Yoda1, 298 EGF), 5 experiments, 3 siRNA transfections. Scale bar = 20μm. Error bars = median±interquartile range. ns= non-significant, * $p<0.05$, **** $p< 0.0001$, one-way ANOVA followed by Kruskal-Wallis post-hoc test with Dunn's correction for multiple comparisons.

## EGFR kinase activity is dispensable for Piezo1-triggered EGFR endocytosis

Both canonical ligand-dependent EGFR activation (phosphorylation and internalization) or its transactivation by other transmembrane proteins, by calcium signaling, or by mechanical forces relies on ligand-receptor interaction and EGFR autophosphorylation of cytoplasmic tyrosines by its kinase domain (4–7, 28). Given that Piezo1 is a transmembrane protein that mediates calcium influx activated by mechanical forces (11), we tested if Piezo1-dependent EGFR signaling requires receptor autophosphorylation. Preincubation with the EGFR kinase inhibitor PD153035 (28, 43) did not alter EGFR internalization in response to Yoda1, but did in response to EGF (Fig.2A, B, C). In addition, Yoda1 treatment did not increase EGFR phosphorylation at Y1173 or Y1068, two major autophosphorylation sites (25, 35, 38, 39, 43) in western blots (Fig.2D, E). Based on our images, we conclude that EGFR internalization after Piezo1 activation does not require EGFR autophosphorylation or its phosphorylation of the endocytic machinery (26, 41). Moreover, our western blots show that

EGFR endocytosis after Piezo1 activation does not involve canonical EGFR tyrosine phosphorylation. With this in mind, we explored additional mechanisms of EGFR regulation.

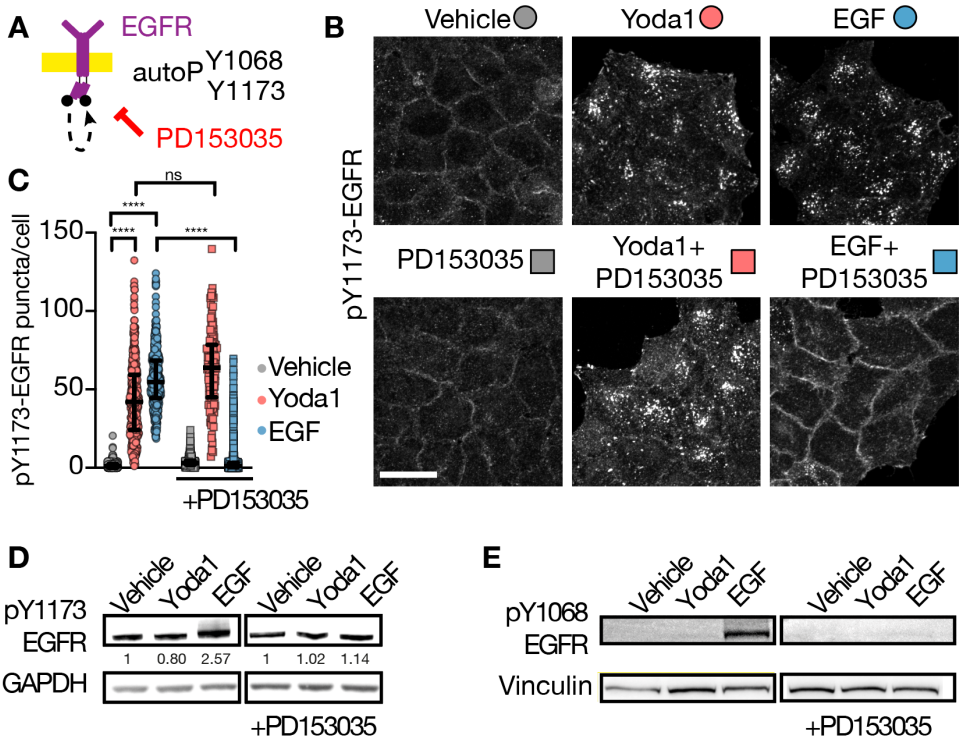


**Figure 2. EGFR kinase activity and tyrosine phosphorylation are dispensable for Piezo1-triggered EGFR endocytosis**
(A) Schematic of the experimental set-up. (B) Representative maximum intensity projections of pY1173-EGFR stainings in HeLa cells treated for 15min with vehicle, 10μM Yoda1 or 10ng/mL EGF with or without 1 μM PD153035 (EGFR kinase inhibitor). (C) Counts of pY1173-EGFR puncta per cell after the indicated treatments. Each symbol represents a cell. Vehicle: 2725, Yoda1: 860, EGF: 1766; PD: 2136, Yoda1+PD: 405, EGF+PD: 2410, 6 experiments. (D, E) Representative western blots of Y1173- and pY1068-EGFR. GAPDH and Vinculin used as loading controls. Scale bar= 20μm. Error bars = median±interquartile range. ns = non-significant, **** $p < 0.0001$ in one-way ANOVA followed by Kruskal-Wallis post-hoc test with Dunn's correction for multiple comparisons.

## Src family and p38 kinases are essential for Piezo1-triggered EGFR endocytosis

Cell-matrix adhesion regulates EGFR via the Src Family Kinases (SFK) (3, 35) and can bypass EGFR kinase activity (36). HeLa cell pre-treatment with the SFK inhibitor PP2 suppressed Yoda1-induced pY1173-EGFR internalization, while it did not affect responses to EGF (Fig.3A-C). This shows that EGFR endocytosis in response to Yoda1 requires SFK activity. Although adhesion-dependent EGFR signaling requires SFK-dependent phosphorylation of EGFR on Y1068 (36), we found that Yoda1 does not alter pY1068-EGFR levels (Fig.3E). Therefore, we investigated other non-canonical mechanisms of EGFR endocytosis.

p38-dependent non-canonical phosphorylation of serine residues 1046 and 1047 of EGFR (pS1046/1047-EGFR) recruits the endocytic machinery and internalizes EGFR, including ligand-unbound or kinase dead receptors (40, 43–46). Because Piezo1 can activate p38 (47), we tested if p38 kinase could mediate Piezo1-dependent EGFR endocytosis by inhibiting p38 with SB202190. SB202190 suppressed EGFR endocytosis in response to Yoda1, but not EGF (Fig.3A, B, C). Western blots show pS1046/1047-EGFR levels increase in response to Yoda1 but not to EGF, and inhibiting SFK with PP2 or of p38 with SB202190 suppressed this increase (Fig.3L). We conclude that Piezo1

activation leads to SFK- and p38-dependent EGFR phosphorylation at serine 1046 and 1047 to drive non-canonical receptor endocytosis.

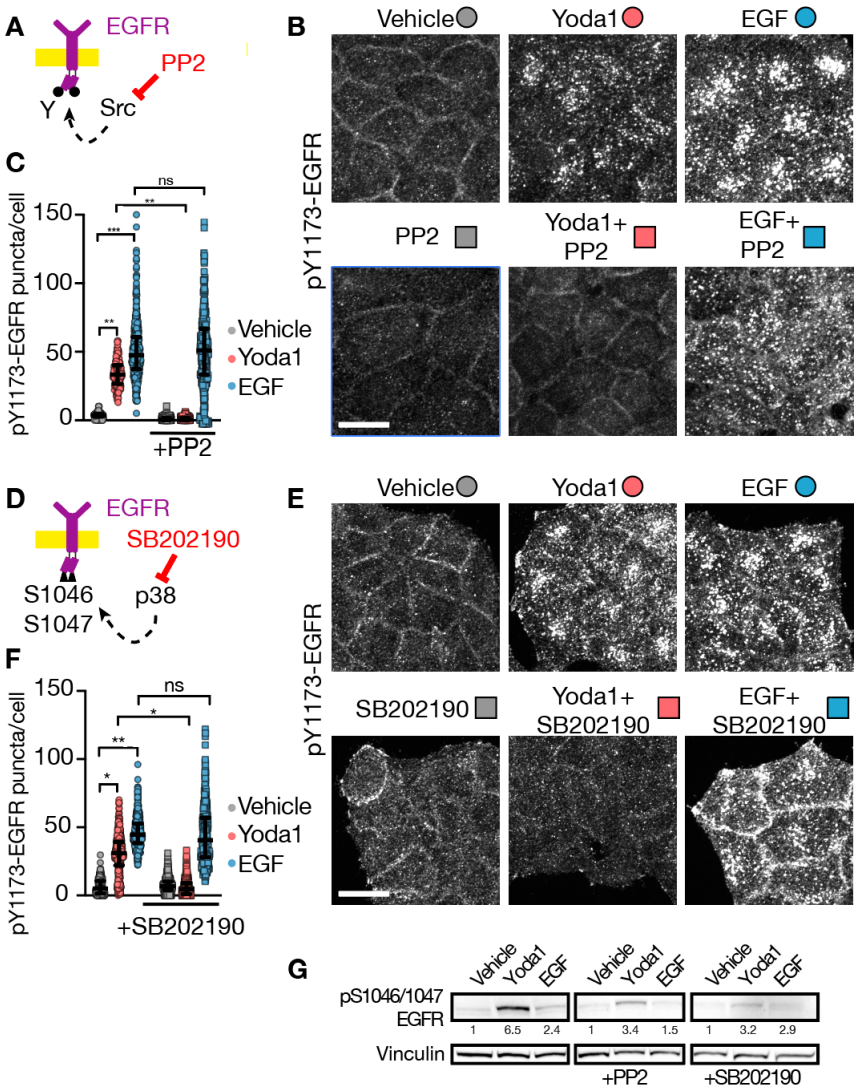


**Figure 3. Non-canonical EGFR serine phosphorylation by an SFK-p38 axis in response to Piezo1 activation.**
(A, D) Schematic of the experimental set-ups. (B, E) Representative maximum intensity projections of pY1173-EGFR stainings in HeLa cells treated for 15min with vehicle, 10μM Yoda1 or 10ng/mL EGF with or without 200nM PP2 (SFK inhibitor, B), or 10 μM SB202190 (p38 inhibitor, E). (C, F) Counts of pY1173-EGFR puncta per cell after the indicated treatments. Each symbol represents a cell. Vehicle: 1143, Yoda1: 717, EGF: 32, PP2: 1694, Yoda1+PP2: 887, EGF+PP2: 829, 6 experiments (C); Vehicle: 867, Yoda1: 1125, EGF: 1544, SB: 948, Yoda1+SB: 1358, EGF+SB: 1016, 3 experiments (F); (G) Representative western blots of pS1046/1047-EGFR. Scale bar= 20μm. Error bars = median±interquartile range. ns = non-significant, * $p<0.05$, ** $p<0.01$, *** $p<0.001$ one-way ANOVA followed by Kruskal-Wallis post-hoc test with Dunn's correction for multiple comparisons.

## Functional EGFR internalization in response to Piezo1 activation leads to different nuclear signals

Canonical EGFR signaling starts at the plasma membrane, but continues as the receptor and its binding partners progress along the endocytic pathway until their eventual recycling to the plasma membrane or lysosomal degradation (1, 2, 26). ERK1/2 MAPK activation is a hallmark of EGFR signaling, and its

spatiotemporal dysregulation underlies many steps of tumorigenesis (1, 32). Western blots showed similar levels of (active) phosphorylated ERK1/2 (pERK1/2) after 15-minute treatments with Yoda1 or EGF (Fig.4A, left lanes). The EGFR kinase inhibitor PD153035 suppressed pERK1/2 increases by EGF, but only partially inhibited those by Yoda1 (Fig.4A, center lanes). The SFK inhibitor PP2 reduced Yoda1- and EGF-induced pERK1/2 (Fig.4A, right lanes). These results demonstrate that both stimuli activate ERK1/2 via EGFR kinase and SFK, but in different proportions: EGF largely depends on EGFR kinase, whereas Piezo1 predominantly depends on SFKs. Amplitude, duration, and location determine pERK1/2 signaling outcomes (32, 48). Interestingly, pERK1/2 accumulates within nuclei in response to 15min of Yoda1 but not EGF treatment (Fig.4B, C). Therefore, despite triggering similar pERK1/2 levels, Piezo1- and EGF-dependent EGFR internalization have different signaling outcomes. As in previous experiments, siPiezo1 cells did not respond to Yoda (Fig.S2A, B), confirming that Yoda1 relies on Piezo1.

One key cellular response to pERK1/2 signaling is activation of the Immediate Early Genes (IEG), including FOS and JUN (1, 32). The duration and strength of nuclear pERK1/2 signaling regulates downstream expression dynamics of the transcription factor FOS, which ultimately drives cell proliferation, differentiation, and transformation (1, 32, 49). Stainings after 2h treatments showed clear nuclear accumulation of FOS and phosphorylated JUN (pJUN) in response to Yoda1, but not EGF (Fig.4 D, E). Yoda1 effects were lost in siPiezo1 cells (Fig.S2C, D). FOS and JUN form the dimeric transcription factor AP-1, a key driver of oncogenic growth, dissemination, and distant organ colonization. In turn, AP-1 cooperates with YAP, a transcriptional regulator with essential roles in (de)differentiation, regeneration, and malignancy, in response to mechanical signals (12, 14, 50–52), including Piezo channel activation(18, 19). Importantly, 2h treatments with Yoda1, but not EGF (Fig.4F, G), caused nuclear YAP accumulation, an effect lost in siPiezo1 cells (Fig.S2E, F). These results show that Piezo1 activation triggers sustained nuclear accumulation of AP-1 (JUN and FOS) and their mechanosensitive interactor YAP.

Tissue damage initiates mechanical signals that activate YAP via SFKs (51, 53). These signals are dispensable for homeostatic epithelial turnover, but essential for reprogramming differentiated cells for regeneration (51, 53, 54) and tumorigenesis (52). Differentiated cells can also be reprogrammed into lineage-restricted stem cells exogenously by pulses of forced YAP expression (50, 55). To investigate Piezo1-dependent activation of EGFR and YAP in an tissue context, we used ex vivo cultured mouse lung slices, which have been used previously to study EGFR activation by mechanical stimuli (7). pY1173-EGFR levels were negligible in control samples, whereas 15-min treatments with Yoda1 significantly increased the number of intracellular pY1173-EGFR puncta in airway cells (Fig.4H). In addition, Yoda1 treatments for 24h, 48, or 72h increased the number of airway cells positive for nuclear YAP and the cycling cell marker Ki67, which were negligible in control samples (Fig.4I). Our lung slice experiments show that the Piezo1-EGFR and Piezo1-YAP dependent signaling are conserved *ex vivo and* suggest that Piezo1 activation can promote cell cycle re-entry of differentiated cells.

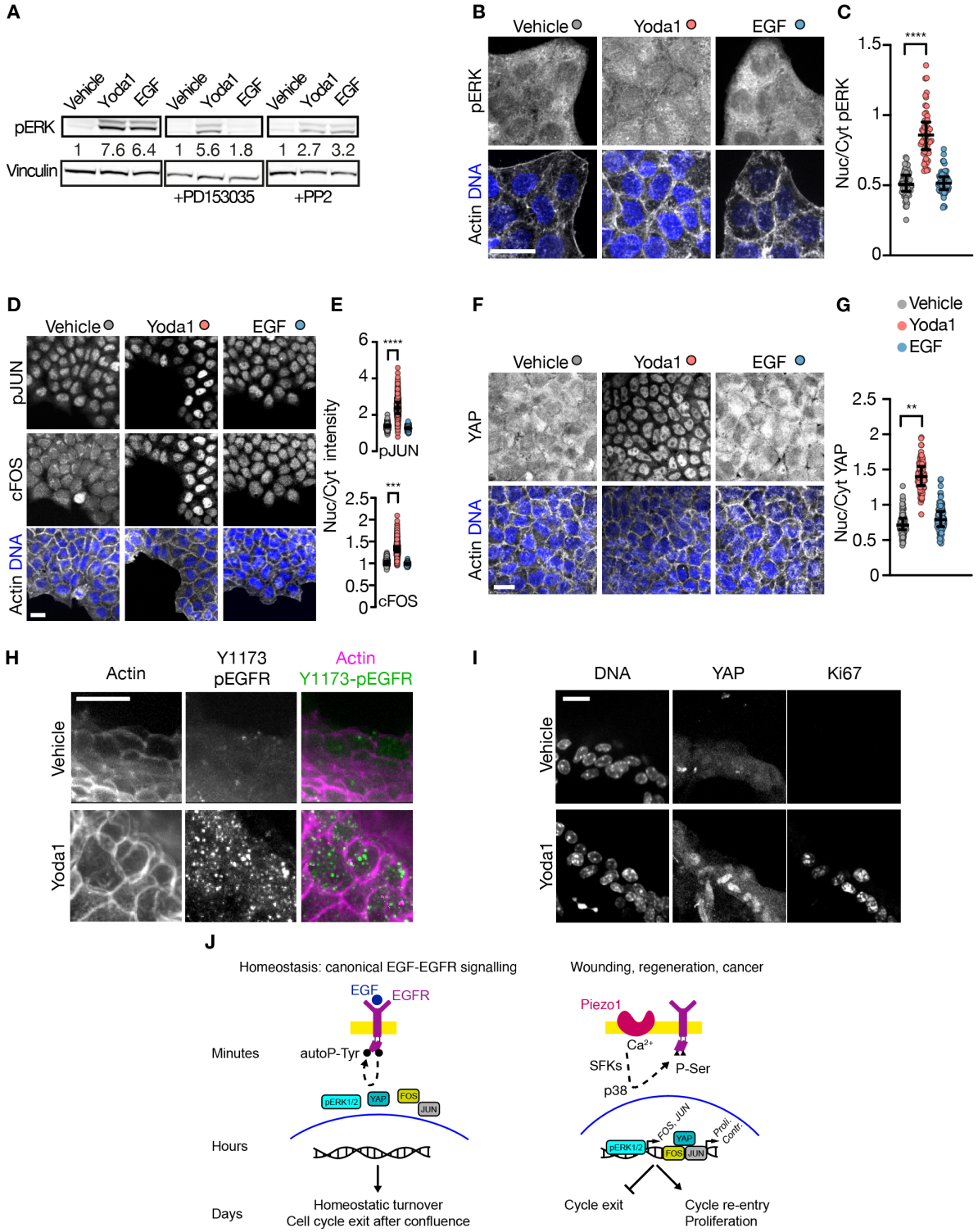


**Figure 4. Different downstream signalling in response to Piezo1 activation.**

Representative western blot (A) and immunostainings (B) of pERK1/2 after 15min of the indicated treatments. Vinculin used as a loading control in A, DNA and Actin shown as spatial references in B. (C) Quantification of the nuclear vs cytoplasmic enrichment of pERK1/2 signal. (D, F) Representative immunostainings of pJUN and FOS (D) or YAP (F) after 2h of the indicated treatments. DNA and Actin shown as spatial references. (E, G) Quantification of the nuclear vs cytoplasmic enrichment of pJUN and FOS (E) or YAP (G) signal. (H, I) Representative immunostainings of pY1173-EGFR after 15min or of YAP and Ki67 after 48h of the indicated treatments. Actin and DNA used as spatial references. (J) Model schematic. Each symbol in C, E, and G represents a cell. Vehicle: 91 (C), 3538 (E), 177 (G); Yoda1: 152 (C), 2543 (E), 301 (G); EGF: 160 (C), 3110 (E), 283 (G). Scale bar= 20μm. Error bars = median±interquartile range. ** $p < 0.01$, *** $p<0.001$, **** $p < 0.0001$ in one-way ANOVA followed by Kruskal-Wallis post-hoc test with Dunn's correction for multiple comparisons.

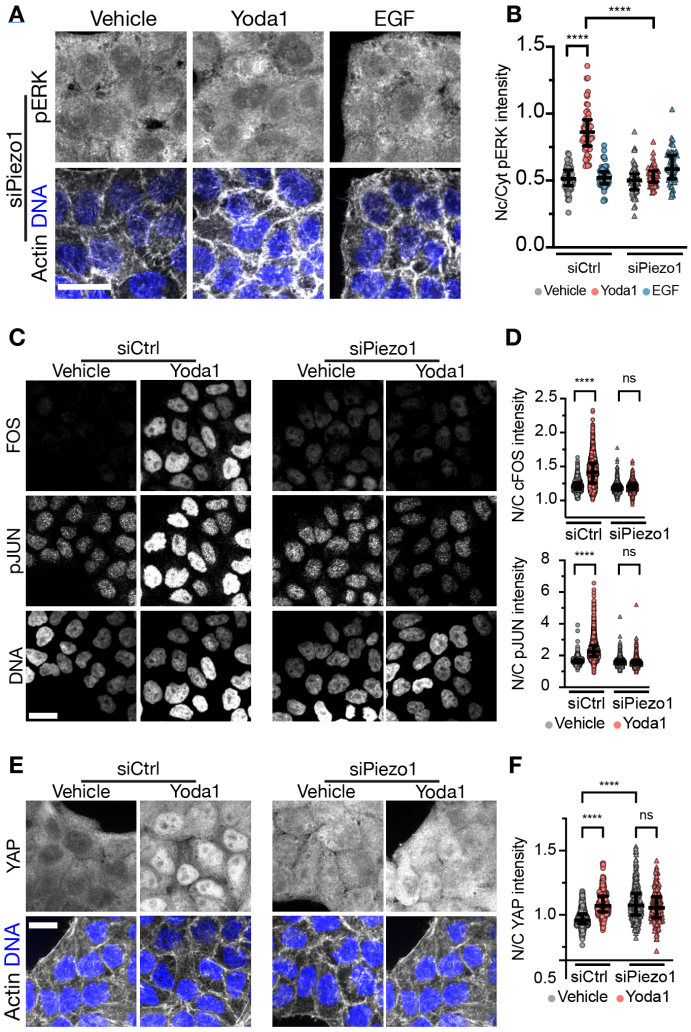


**Figure S2. Piezo1 knockdown suppresses nuclear responses to Yoda1.**

(A, C, E) Representative immunostainings of pERK1/2 (A) after 15min or FOS, pJUN (C) and YAP (E) after 2h of the indicated treatments. DNA and Actin shown as spatial references. (B, D, F) Quantification of the nuclear vs cytoplasmic enrichment of pERK1/2 (B), FOS, pJUN (D) and YAP (F) signal. Each symbol in B, D, and F represents a cell. siControl (Vehicle: 91 (C), 11088 (D), 420 (F); Yoda1: 152 (B), 2299 (E), 362 (F); EGF: 160 (C)), siPiezo1 (Vehicle: 146 (B), 1288 (D), 318 (F); Yoda1: 194 (B), 1449 (D), 209 (F). Scale bar= 20μm. Error bars = median±interquartile range. ** $p< 0.01$, *** $p<0.001$, **** $p< 0.0001$ in one-way ANOVA followed by Kruskal-Wallis post-hoc test with Dunn's correction for multiple comparisons.

## Discussion

We show that Piezo1 activates EGFR endocytosis differentially to the canonical EGF-dependent pathway (Fig.4J). During steady state cell turnover, EGF controls EGFR activation via tyrosine phosphorylation, receptor internalization, and cytoplasmic ERK activation. Here, we find that acute Piezo1-dependent activation of EGFR signals SFK/p38/ nuclear ERK to transcribe early intermediate genes (FOS, JUN) and YAP to promote cell cycle entry. In this way, the same receptor can interpret different inputs to relay separate outcomes. Cell proliferation, death, and differentiation are controlled by paradoxical signaling, contributing to sub-population balance in the immune system (56) or to homeostatic cell density maintenance in the epithelium (21, 22). Remarkably, Piezo1 and ERK both contribute to paradoxical signaling controlling cell number homeostasis, where their differential activation triggers opposite responses, depending on the mechanical and mutational context: cell extrusion and death upon crowding, or rapid cell division after stretch (21, 22, 57).

Previous reports have shown that transmembrane proteins like integrins (3) or GPCRs (4) or mechanical stimuli transactivate EGFR (7, 25, 29, 30, 33, 36). However, these activation modes rely on SFK-dependent metalloprotease activation and production of EGF to bind EGFR and promote canonical signaling via receptor tyrosine autophosphorylation (3, 4, 7, 28). Instead, we find that Piezo1 activates EGFR signaling via non-canonical serine 1046/1047 EGFR phosphorylation, independent of tyrosine autophosphorylation. We also identify a new essential role for SFKs in ligand-independent EGFR signaling. This could expand previous findings that SFKs activate p38 in response to radiation and to *Candida* infections to promote survival and infection clearance (58, 59), respectively, via ligand independent EGFR signaling. Together, these observations propose p38 as a general transactivator of EGFR in response to stressors, with a pro-survival and regenerative signaling output different from ligand-induced canonical responses.

Our data showing EGFR activation by Piezo1 suggests a new important signaling axis for regenerative and tumorigenic responses that may explain other findings in cancer. In gliomas, Piezo1 expression and activity correlate with malignancy and EGFR signaling (20, 60). SFKs, p38, and EGFR are frequently overexpressed and potentiate each other in many cancers, causing resistance to EGFR tyrosine kinase inhibitors and poor prognosis (27, 61). Notably, internalization of non-phosphorylated or kinase-defective EGFR via p38-dependent non-canonical serine phosphorylation contributes to chemoresistance by increased cell survival (43, 62, 63). Given the importance of non-canonical EGFR signaling in cancer, it is tempting to speculate that EGFR tyrosine kinase inhibitor resistance in some cancers may stem from mechanical EGFR signaling via the Piezo1-SFK-p38 axis. Thus, targeting this axis could provide therapeutic benefit for kinase inhibitor-resistant tumors.

Importantly, using ex vivo mouse lung slices, an established model for EGFR research (7), we find that Piezo1 activation with Yoda1 increases intracellular pY1173-EGFR puncta, consistent with it endocytosis, in airway cells. Additionally, Piezo1-dependent activation of cell cycle re-entry occurred following nuclear YAP accumulation in lung slices. Given that YAP activation can de-differentiate cells into lineage-restricted stem cells (50) and increase organ size (55), Yoda1 might provide a simple method to obtain tissue-specific stem cells in culture or promote tissue growth.

Our work identifies Piezo1 as a missing link required to mechanically activate EGFR via SFK/p38 kinases and serine phosphorylation. This axis is independent of EGFR tyrosine phosphorylation and kinase function and results in regenerative/oncogenic signaling rather than homeostatic cell turnover control. Given the roles of mechanics in regeneration, oncogenesis, and the increased prevalence of tyrosine kinase inhibitor chemoresistance, our discovery may reveal insight into EGFR signaling during repair and malignancy.

## Materials & Methods

Unless noted, reagents were from ThermoFisher.

### Cell culture

Non-verified HeLa cells were grown in DMEM (31966021) with 10% FBS (10270106) and 1% Pen/Strep (15070063) in a cell culture incubator at 37°C with 5% $CO_2$. For all experiments, cells were seeded in growth medium. After 24h, growth medium was washed and replaced by starvation medium (DMEM+1%Pen/Strep, prepared without FBS) for 24h before cell treatment. All cells tested negative for Mycoplasma contamination in periodic PCR tests (Sartorius, 20-700-20).

### siRNA transfection

The day after seeding, 20%-40% confluent cells were transfected with Lipofectamine RNAiMax (13778) and OptiMEM (31985062) following manufacturer's instructions. siRNA pool (Horizon Discovery, siControl: D-001810-10-50, siPIEZO1: L-020870-03-0050) final concentration was 10nM. After 72h, cells were trypsinized and seeded on glass coverslips in growth medium before starvation and treatment.

### Compounds

24h after serum starvation, cells were treated with DMSO (276855), 10μM Yoda1 (Tocris, 5586, reconstituted in DMSO) or 10ng/mL EGF (Peprotech, 400-25, reconstituted in deionized water) for desired durations. Experiments involving inhibitors included a 30-min treatment pre-treatment with 1μM PD153035 (Sigma, SML0564), 200nM PP2 (Sigma, P0042), or 10 μM SB202190 (Abcam, ab120638), all reconstituted in DMSO. All treatments were prepared recycling medium used to starve cells.

### Western blot

Cells were seeded on 10cm culture plates and starved and treated when 60-70% confluent. After treatment, plates were placed on ice, washed twice with ice-cold PBS, and lysed in 250μL/plate of RIPA buffer (89901) supplemented with EDTA and protease (78430) and phosphatase (Merck, 524625) inhibitor cocktails. After 1min of incubation on ice, plates were scraped and the lysate placed in tubes, followed by 30-min incubation in ice, vortexing every 5 minutes. Lysates were then centrifuged at 13000 rpm for 10 min at 4°C. The resulting supernatants were placed in new tubes and their protein content quantified with a BCA kit (23225). 50μg grams of protein adjusted to 10 μL in RIPA and dying (B0007) buffers were denatured at 95°C for 10 min, spun down, supplemented with a sample reducing buffer (B0004), and loaded in 4-12% Bis-Tris gels (NW04120BOX). A well with 5 μL of a pre-stained protein standard (LC5925) was used to track protein separation during electrophoresis at 120V for 1.5h in MOPS SDS buffer (B0001). Proteins were then transferred to nitrocellulose membranes (IB23002) with a dry transfer device (IB21001) at 25V for 8min. Membranes were blocked for 1h at room temperature (RT) with 5% BSA (for phosphorylated targets) or with 5% non-fat powder milk, both prepared in 0.1% Tween-20 (Sigma, P137) TBS (TTBS). After overnight primary antibody incubation and 3 5min-washings, membranes were incubated at RT for 1h with secondary antibodies followed by 3 additional 5min-washings, 1-min incubation with ECL substrate (32209) and imaging. Band density was later quantified with the Analyze/Gels tool in Fiji (64). In some cases, membranes were then stripped and re-blotted following manufacturer's instructions (Sigma, 2500). TTBS was used for all washings.

### Calcium imaging

Cells grown on glass coverslips were loaded with 4.5 µM of the calcium-sensitive dye Calbryte-520AM (AAT Bioquest, 20651, reconstituted in DMSO) for 30min in the cell culture incubator (37°C, 5% CO2), followed by washing and 30min of additional incubation for AM cleavage and dye equilibration. Coverslips were then mounted on a recording chamber (Warner Instruments, 642420) and intracellular calcium levels were imaged at RT using a 20x air objective, 2x2 binning, and GFP-compatible epifluorescence settings. Fluobrite DMEM (A1896701) supplemented with 20mM HEPES (15630080) was used to prepare all solutions. A peristaltic pump (Fisher Scientific, 16609762) connected to the recording chamber exchanged solutions.

### Antibodies-Staining

**Primaries:** pY1173-EGFR (1/250, R&D Systems, AF1095), EEA1 (1/250, BD, 610457), phospho-ERK (1/200, CST, 4370S), YAP (1/200, SCBT, sc-101199), phospho-cJUN(1:200, Abcam, ab32385), cFOS (1/200, SCBT, sc-166940), Ki67 (1/100, Abcam, ab16667). For mouse lung slices, 1/100 was used. All antibodies were incubated overnight at 4°C in 1% BSA (A7906-100G) in PBS (14190250). **Secondaries**: 1/250 (cell culture) or 1/100 (lung slices) Alexa Fluor (AF)-conjugated 488 Anti-Rabbit (A11008) and 594 Anti-Mouse (A11005), supplemented with 1/500 AF647 Phalloidin (A22287) and 30 µg/ml Hoechst (62249) were prepared in 1% BSA (A7906-100G) in PBS (14190250) and incubated 1h at RT.

### Antibodies-Western Blot

**Primaries:** pY1173-EGFR (R&D Systems, AF1095), pY1068-EGFR (CST, 3777S), pS1046/S1047-EGFR (Abcam, ab76300), pERK1/2 (CST, 4370S) all 1/1000 in 5% BSA-TTBS; Vinculin (700062), GAPDH (Abcam, ab8245) 1/1000 in 5% fat free powder milk-TTBS. Incubated overnight at 4°C inside Falcon tubes with constant rotation. **Secondary:** HRP-conjugated secondary anti-Rabbit antibody (65-6120) diluted 1:2500 in 5% non-fat powder milk-TTBS. Incubated 1h at RT.

### Lung slice obtention, treatment, and staining

Mouse lung slices were obtained using an adaption of an established protocol(65) approved according to the Animal Scientific Procedures Act. Mice were killed by inhalation of $CO_2$ followed by cervical dislocation. After opening the chest cavity, a 20Gx1.25 in canula was inserted in the trachea through a small incision and used to inflate the lungs with 2% low melting agarose (Fisher, BP1360, 2% in HBSS (14025)). After excision and washing in PBS, the lobes were separated and individually embedded in 4% low melting agarose. After casting on ice, a Leica VT1200S vibratome was used to cut 200 µm-thick slices. Slices were washed and incubated overnight in DMEM/F-12(11320033) with 10% FBS and 1% Pen/Strep in the cell culture incubator. The next morning, slices were individually transferred to a 24-well plate and treated with DMSO, or 10 µM Yoda1. After the indicated times, treatments were aspirated, and slices washed thrice with PBS and fixed with 4% PFA overnight at 4°C. After 2 30-min washings, slices were blocked in 0.1% Triton X-100 and 1% BSA. Primary and secondary antibodies were consecutively incubated overnight at 4°C before incubation with 1/1000 DAPI for 20min and mounting in Prolong Gold (P36930). 0.5% Triton X-100 was used for 3 30-min washings between incubations. All solutions prepared in PBS.

### Fixed cell staining

After treatment, cells grown on glass coverslips were fixed in 4% PFA (28908) for 20min at 37°C, permeabilized with 0.5% Triton X-100 (Sigma, X-100) for 5min at RT and stained with primary (overnight, 4°C) and secondary (1h, RT) antibodies. Coverslips were mounted with Fluoromount-G (00-4958-02). All solutions were prepared and washed with PBS.

### Imaging

Samples were imaged at 1μm-thick Z displacements through 20X and 40X air and 60X oil objectives of a Nikon Eclipse Ti2-E microscope with a Yokogawa CSU-W1 spinning disk system coupled to an Andor DU-888 camera, and a Toptica multi-laser bed. Settings remained unchanged between conditions.

### Image analysis

pY1173 internalization

Maximum Intensity Projections were built from raw ND2 files in Fiji. Next, Cell Profiler (66) was used to sequentially 1) segment nuclei using the DNA channel, 2) segment cells on the actin channel using nuclei as seeds, 3) generate masks of the cytoplasm after shrinking segmented cells to omit cell boundaries, 4) enhance speckles in the pY1173-EGFR image using a feature size of 10, 5) segment speckles for counting, and 6) export data.

Nuclear translocation of YAP, cFOS, and pJUN

Background, intra-, and juxta- nuclear ROIs were manually drawn with Fiji using the mid-height image of each Z-stack. The median intensity value of each ROI was measured and exported to a CSV file later used for background subtraction and Nuclear/Cytoplasmic ratio calculation in RStudio or Excel.

### Statistics

All graphs and statistical analyses were done with Prism 9.3.1 (GraphPad Software). Data are presented as median±interquartile range. Given that data distribution was not gaussian, the statistical significance of the differences between treatments was assessed with one-way ANOVA followed by Kruskal-Wallis post-hoc test with Dunn's correction for multiple comparisons, as suggested by the software. The threshold for statistical significance was $p<0.05$.

## Acknowledgements

We thank C. Mulas, M. A. Valverde, and F. X. Real for critical reading of the manuscript, F. Fore and D.C. Bagley for help with mouse work, and E. Ortiz-Zapater, M. Rigau de Llobet, and the members of the Rosenblatt lab for their patience, technical input, and helpful discussions.

## Competing interests and funding

The authors declare no competing interests. C.P.-P. is the recipient of a Long-Term Fellowship (LT000654/2019-L) from the Human Frontier Science Program organization and a Marie Skłodowska-Curie Fellowship (898067) from the European Union's Horizon 2020 research and innovation program. This research was funded in part by a Wellcome Trust Investigator Award (221908/Z/20/Z), a Cancer Research UK (DRCNPG-May21\100007), an Academy of Medical Sciences Professorship (APR2\1007), and a King's College London start-up grant to JR. For open access, the authors have applied a CC BY public copyright license to any Author Accepted Manuscript version arising from this submission.

## Author contributions

C.P.-P. designed and performed research, contributed reagents/analytic tools, analyzed data, and wrote the paper; J.R. discussed research and edited the paper.

## References


1. R. Avraham, Y. Yarden, Feedback regulation of EGFR signalling: decision making by early and delayed loops. *Nat. Rev. Mol. Cell Biol.* **12**, 104–117 (2011).
2. M. A. Lemmon, J. Schlessinger, Cell Signaling by Receptor Tyrosine Kinases. *Cell* **141**, 1117–1134 (2010).
3. L. Moro, *et al.*, Integrins induce activation of EGF receptor: role in MAP kinase induction and adhesion-dependent cell survival. *EMBO J.* **17**, 6622–6632 (1998).
4. N. Prenzel, *et al.*, EGF receptor transactivation by G-protein-coupled receptors requires metalloproteinase cleavage of proHB-EGF. *Nature* **402**, 884–888 (1999).
5. L. B. Rosen, M. E. Greenberg, Stimulation of growth factor receptor signal transduction by activation of voltage-sensitive calcium channels. *Proc. Natl. Acad. Sci.* **93**, 1113–1118 (1996).
6. B. Sullivan, *et al.*, Mechanical disruption of E-cadherin complexes with epidermal growth factor receptor actuates growth factor–dependent signaling. *Proc. Natl. Acad. Sci.* **119**, e2100679119 (2022).
7. D. J. Tschumperlin, *et al.*, Mechanotransduction through growth-factor shedding into the extracellular space. *Nature* **429**, 83–86 (2004).
8. M. Abercrombie, J. E. Heaysman, Observations on the social behaviour of cells in tissue culture. I. Speed of movement of chick heart fibroblasts in relation to their mutual contacts. *Exp. Cell Res.* **5**, 111–131 (1953).
9. J. Folkman, A. Moscona, Role of cell shape in growth control. *Nature* **273**, 345–349 (1978).
10. F. M. Watt, P. W. Jordan, C. H. O'Neill, Cell shape controls terminal differentiation of human epidermal keratinocytes. *Proc. Natl. Acad. Sci.* **85**, 5576–5580 (1988).
11. B. Coste, *et al.*, Piezo1 and Piezo2 Are Essential Components of Distinct Mechanically Activated Cation Channels. *Science* **330**, 55–60 (2010).
12. S. Dupont, *et al.*, Role of YAP/TAZ in mechanotransduction. *Nature* **474**, 179–183 (2011).
13. R. Latorre, I. Díaz-Franulic, Profile of David Julius and Ardem Patapoutian: 2021 Nobel Laureates in Physiology or Medicine. *Proc. Natl. Acad. Sci.* **119**, e2121015119 (2022).
14. K.-I. Wada, K. Itoga, T. Okano, S. Yonemura, H. Sasaki, Hippo pathway regulation by cell morphology and stress fibers. *Development* **138**, 3907–3914 (2011).
15. W.-C. Hung, *et al.*, Confinement Sensing and Signal Optimization via Piezo1/PKA and Myosin II Pathways. *Cell Rep.* **15**, 1430–1441 (2016).
16. J. Carrillo-Garcia, *et al.*, The mechanosensitive Piezo1 channel controls endosome trafficking for an efficient cytokinetic abscission. *Sci. Adv.* **7**, eabi7785 (2021).
17. J. Li, *et al.*, Piezo1 integration of vascular architecture with physiological force. *Nature* **515**, 279–282 (2014).
18. C. Pardo-Pastor, *et al.*, Piezo2 channel regulates RhoA and actin cytoskeleton to promote cell mechanobiological responses. *Proc. Natl. Acad. Sci.* **115**, 1925–1930 (2018).
19. M. M. Pathak, *et al.*, Stretch-activated ion channel Piezo1 directs lineage choice in human neural stem cells. *Proc. Natl. Acad. Sci.* **111**, 16148–16153 (2014).
20. X. Chen, *et al.*, A Feedforward Mechanism Mediated by Mechanosensitive Ion Channel PIEZO1 and Tissue Mechanics Promotes Glioma Aggression. *Neuron* **100**, 799-815.e7 (2018).
21. G. T. Eisenhoffer, *et al.*, Crowding induces live cell extrusion to maintain homeostatic cell numbers in epithelia. *Nature* **484**, 546–549 (2012).
22. S. A. Gudipaty, *et al.*, Mechanical stretch triggers rapid epithelial cell division through Piezo1. *Nature* **543**, 118–121 (2017).
23. B. W. Benham-Pyle, B. L. Pruitt, W. J. Nelson, Mechanical strain induces E-cadherin-dependent Yap1 and -catenin activation to drive cell cycle entry. *Science* **348**, 1024–1027 (2015).
24. Y. Han, *et al.*, Mechanosensitive ion channel Piezo1 promotes prostate cancer development through the activation of the Akt/mTOR pathway and acceleration of cell cycle. *Int. J. Oncol.* (2019) https:/doi.org/10.3892/ijo.2019.4839 (July 30, 2019).

25. P. E. Farahani, *et al.*, Substratum stiffness regulates Erk signaling dynamics through receptor-level control. *Cell Rep.* **37**, 110181 (2021).
26. S. Sigismund, *et al.*, Clathrin-mediated internalization is essential for sustained EGFR signaling but dispensable for degradation. *Dev. Cell* **15**, 209–219 (2008).
27. S. Belli, *et al.*, c-Src and EGFR Inhibition in Molecular Cancer Therapy: What Else Can We Improve? *Cancers* **12**, 1489 (2020).
28. N. Hino, *et al.*, ERK-Mediated Mechanochemical Waves Direct Collective Cell Polarization. *Dev. Cell* **53**, 646-660.e8 (2020).
29. H. Iwasaki, S. Eguchi, H. Ueno, F. Marumo, Y. Hirata, Mechanical stretch stimulates growth of vascular smooth muscle cells via epidermal growth factor receptor. *Am. J. Physiol. Heart Circ. Physiol.* **278**, H521-529 (2000).
30. J.-H. Kim, A. R. Asthagiri, Matrix stiffening sensitizes epithelial cells to EGF and enables the loss of contact inhibition of proliferation. *J. Cell Sci.* **124**, 1280–1287 (2011).
31. S. K. Kuwada, X. Li, Integrin **α**5/**β**1 Mediates Fibronectin-dependent Epithelial Cell Proliferation through Epidermal Growth Factor Receptor Activation. *Mol. Biol. Cell* **11**, 2485–2496 (2000).
32. L. O. Murphy, J. Blenis, MAPK signal specificity: the right place at the right time. *Trends Biochem. Sci.* **31**, 268–275 (2006).
33. V. Umesh, A. D. Rape, T. A. Ulrich, S. Kumar, Microenvironmental Stiffness Enhances Glioma Cell Proliferation by Stimulating Epidermal Growth Factor Receptor Signaling. *PLoS ONE* **9**, e101771 (2014).
34. S. Yano, M. Komine, M. Fujimoto, H. Okochi, K. Tamaki, Mechanical Stretching In Vitro Regulates Signal Transduction Pathways and Cellular Proliferation in Human Epidermal Keratinocytes. *J. Invest. Dermatol.* **122**, 783–790 (2004).
35. L. Moro, *et al.*, Integrin-induced epidermal growth factor (EGF) receptor activation requires c-Src and p130Cas and leads to phosphorylation of specific EGF receptor tyrosines. *J. Biol. Chem.* **277**, 9405–9414 (2002).
36. M. Saxena, *et al.*, EGFR and HER2 activate rigidity sensing only on rigid matrices. *Nat. Mater.* **16**, 775–781 (2017).
37. R. Syeda, *et al.*, Chemical activation of the mechanotransduction channel Piezo1. *eLife* **4**, e07369 (2015).
38. J. Li, C. Ma, Y. Huang, J. Luo, C. Huang, Differential requirement of EGF receptor and its tyrosine kinase for AP-1 transactivation induced by EGF and TPA. *Oncogene* **22**, 211–219 (2003).
39. M. P. Oksvold, E. Skarpen, B. Lindeman, N. Roos, H. S. Huitfeldt, Immunocytochemical Localization of Shc and Activated EGF Receptor in Early Endosomes After EGF Stimulation of HeLa Cells. *J. Histochem. Cytochem.* **48**, 21–33 (2000).
40. M. Perez Verdaguer, *et al.*, Mechanism of p38 MAPK–induced EGFR endocytosis and its crosstalk with ligand-induced pathways. *J. Cell Biol.* **220** (2021).
41. S. Sigismund, *et al.*, Clathrin-independent endocytosis of ubiquitinated cargos. *Proc. Natl. Acad. Sci.* **102**, 2760–2765 (2005).
42. B. J. McHugh, *et al.*, Integrin activation by Fam38A uses a novel mechanism of R-Ras targeting to the endoplasmic reticulum. *J. Cell Sci.* **123**, 51–61 (2010).
43. T. Tanaka, *et al.*, Ligand-activated epidermal growth factor receptor (EGFR) signaling governs endocytic trafficking of unliganded receptor monomers by non-canonical phosphorylation. *J. Biol. Chem.* **293**, 2288–2301 (2018).
44. M. R. Frey, R. S. Dise, K. L. Edelblum, D. B. Polk, p38 kinase regulates epidermal growth factor receptor downregulation and cellular migration. *EMBO J.* **25**, 5683–5692 (2006).
45. S. Vergarajauregui, A. S. Miguel, R. Puertollano, Activation of p38 Mitogen-Activated Protein Kinase Promotes Epidermal Growth Factor Receptor Internalization. *Traffic* **7**, 686–698 (2006).
46. Y. Zwang, Y. Yarden, p38 MAP kinase mediates stress-induced internalization of EGFR: implications for cancer chemotherapy. *EMBO J.* **25**, 4195–4206 (2006).

47. N. M. Blythe, *et al.*, Mechanically activated Piezo1 channels of cardiac fibroblasts stimulate p38 mitogen-activated protein kinase activity and interleukin-6 secretion. *J. Biol. Chem.* **294**, 17395–17408 (2019).
48. P. Wu, P. Wee, J. Jiang, X. Chen, Z. Wang, Differential Regulation of Transcription Factors by Location-Specific EGF Receptor Signaling via a Spatio-Temporal Interplay of ERK Activation. *PLOS ONE* **7**, e41354 (2012).
49. S. D. M. Santos, P. J. Verveer, P. I. H. Bastiaens, Growth factor-induced MAPK network topology shapes Erk response determining PC-12 cell fate. *Nat. Cell Biol.* **9**, 324–330 (2007).
50. T. Panciera, *et al.*, Induction of Expandable Tissue-Specific Stem/Progenitor Cells through Transient Expression of YAP/TAZ. *Cell Stem Cell* **19**, 725–737 (2016).
51. S. Yui, *et al.*, YAP/TAZ-Dependent Reprogramming of Colonic Epithelium Links ECM Remodeling to Tissue Regeneration. *Cell Stem Cell* **22**, 35-49.e7 (2018).
52. F. Zanconato, *et al.*, Genome-wide association between YAP/TAZ/TEAD and AP-1 at enhancers drives oncogenic growth. *Nat. Cell Biol.* **17**, 1218–1227 (2015).
53. K. Taniguchi, *et al.*, A gp130–Src–YAP module links inflammation to epithelial regeneration. *Nature* **519**, 57–62 (2015).
54. J. Cai, *et al.*, The Hippo signaling pathway restricts the oncogenic potential of an intestinal regeneration program. *Genes Dev.* **24**, 2383–2388 (2010).
55. F. D. Camargo, *et al.*, YAP1 Increases Organ Size and Expands Undifferentiated Progenitor Cells. *Curr. Biol.* **17**, 2054–2060 (2007).
56. Y. Hart, U. Alon, The Utility of Paradoxical Components in Biological Circuits. *Mol. Cell* **49**, 213–221 (2013).
57. T. J. Aikin, A. F. Peterson, M. J. Pokrass, H. R. Clark, S. Regot, MAPK activity dynamics regulate non-cell autonomous effects of oncogene expression. *eLife* **9**, e60541 (2020).
58. M.-J. Kim, *et al.*, c-Src-p38 Mitogen-Activated Protein Kinase Signaling Is Required for Akt Activation in Response to Ionizing Radiation. *Mol. Cancer Res.* **6**, 1872–1880 (2008).
59. S.-A. Nikou, *et al.*, The *Candida albicans* toxin candidalysin mediates distinct epithelial inflammatory responses through p38 and EGFR-ERK pathways. *Sci. Signal.* **15**, eabj6915 (2022).
60. W. Zhou, *et al.*, Identification of PIEZO1 as a potential prognostic marker in gliomas. *Sci. Rep.* **10**, 16121 (2020).
61. R. Mora Vidal, *et al.*, Epidermal Growth Factor Receptor Family Inhibition Identifies P38 Mitogen-activated Protein Kinase as a Potential Therapeutic Target in Bladder Cancer. *Urology* **112**, 225.e1-225.e7 (2018).
62. F. Walker, *et al.*, Activation of the Ras/Mitogen-Activated Protein Kinase Pathway by Kinase-Defective Epidermal Growth Factor Receptors Results in Cell Survival but Not Proliferation. *Mol. Cell. Biol.* **18**, 7192–7204 (1998).
63. X. Tan, N. Thapa, Y. Sun, R. A. Anderson, A Kinase-Independent Role for EGF Receptor in Autophagy Initiation. *Cell* **160**, 145–160 (2015).
64. J. Schindelin, *et al.*, Fiji: an open-source platform for biological-image analysis. *Nat. Methods* **9**, 676–682 (2012).
65. K. M. Akram, *et al.*, Live imaging of alveologenesis in precision-cut lung slices reveals dynamic epithelial cell behaviour. *Nat. Commun.* **10**, 1178 (2019).
66. C. McQuin, *et al.*, CellProfiler 3.0: Next-generation image processing for biology. *PLOS Biol.* **16**, e2005970 (2018).

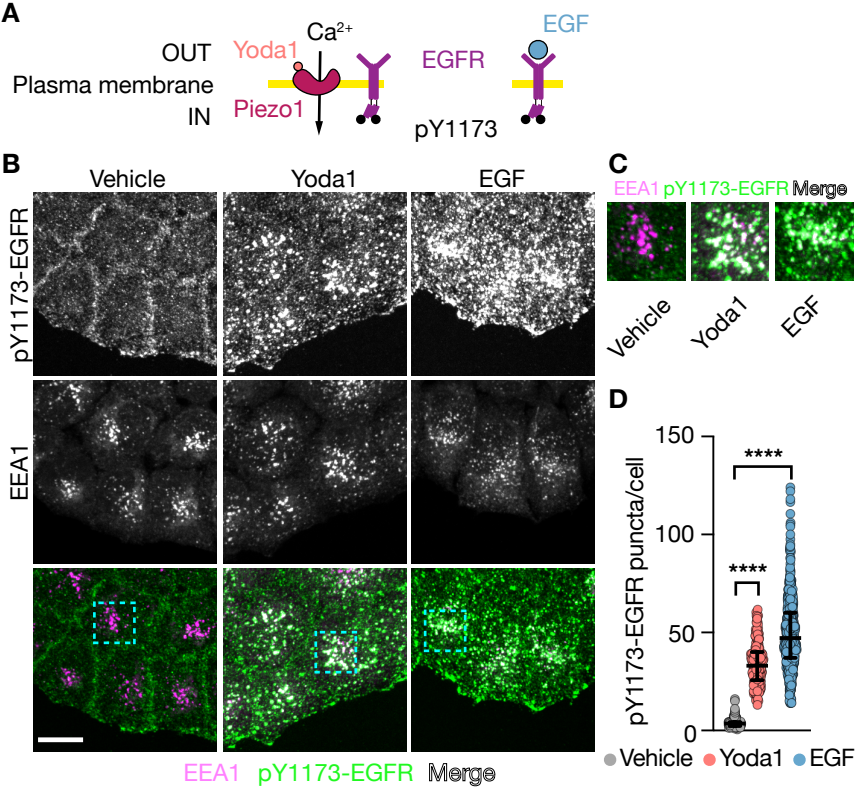
A
OUT
Plasma membrane
IN
Yoda1
Ca2+
Piezo1
EGFR
EGF
pY1173
B
Vehicle
Yoda1
EGF
pY1173-EGFR
EEA1
EEA1 pY1173-EGFR Merge
C
EEA1 pY1173-EGFR Merge
Vehicle
Yoda1
EGF
D
pY1173-EGFR puncta/cell
150
100
50
0
****
****
Vehicle
Yoda1
EGF

Fig.1

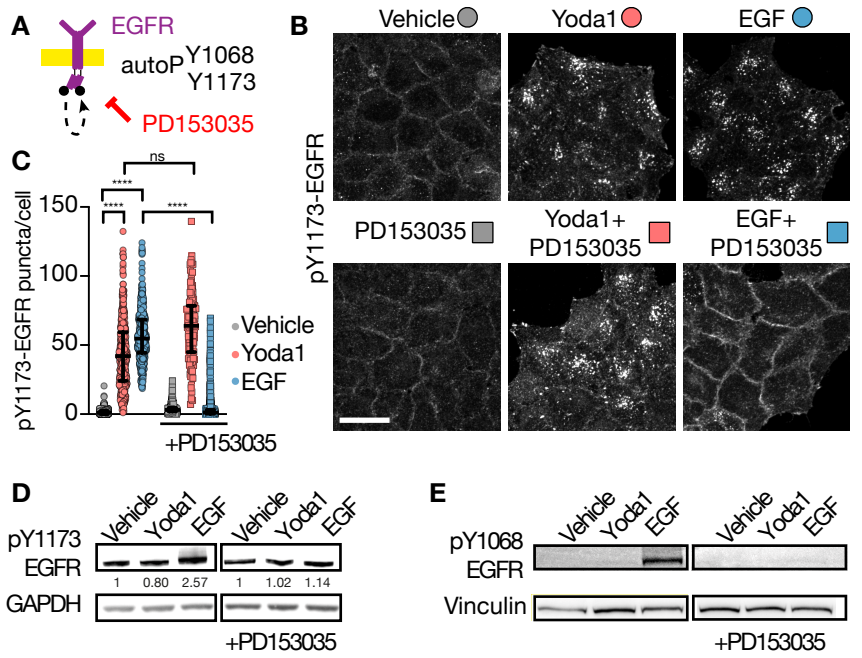
A
EGFR
autoP
Y1068
Y1173
PD153035
B
Vehicle
Yoda1
EGF
pY1173-EGFR
PD153035
Yoda1+
PD153035
EGF+
PD153035
C
pY1173-EGFR puncta/cell
150
100
50
0
ns
****
****
****
Vehicle
Yoda1
EGF
+PD153035
D
Vehicle
Yoda1
EGF
Vehicle
Yoda1
EGF
pY1173
EGFR
1
0.80
2.57
1
1.02
1.14
GAPDH
+PD153035
E
Vehicle
Yoda1
EGF
Vehicle
Yoda1
EGF
pY1068
EGFR
Vinculin
+PD153035

Fig.2

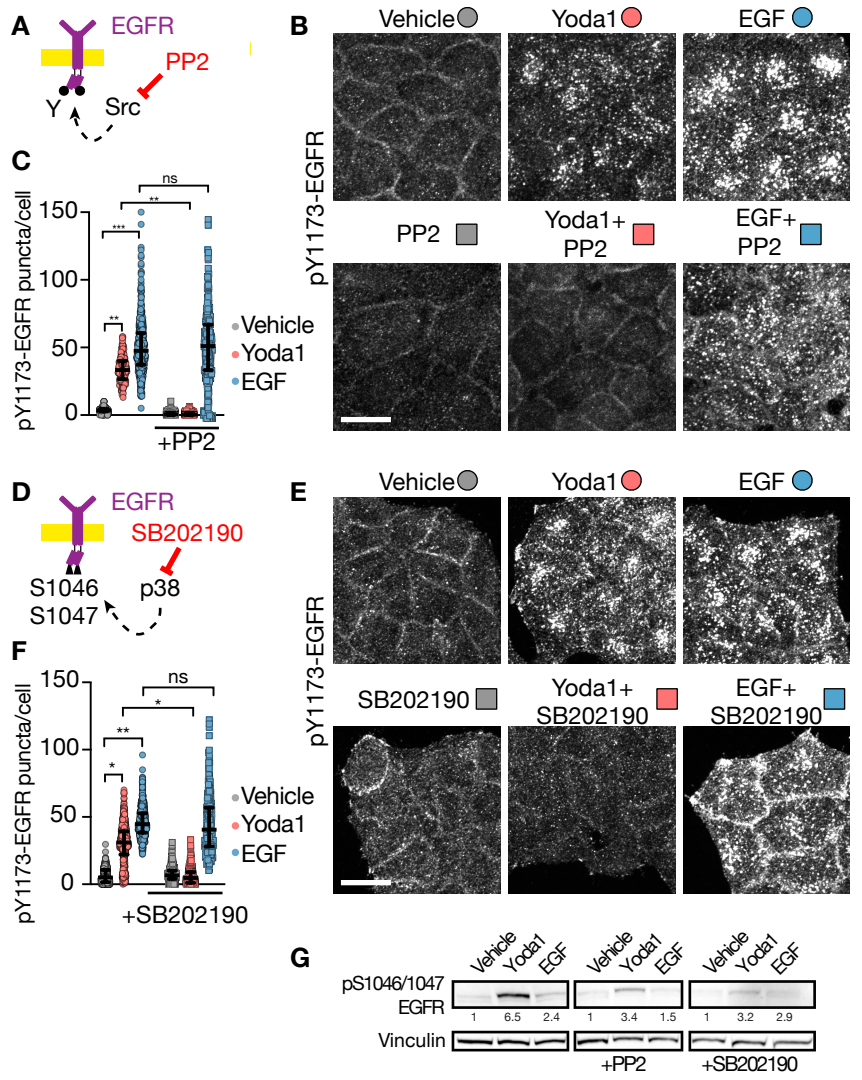
A
EGFR
PP2
Y
Src
B
Vehicle
Yoda1
EGF
pY1173-EGFR
PP2
Yoda1+ PP2
EGF+ PP2
C
pY1173-EGFR puncta/cell
150
100
50
0
ns
**
***
**
Vehicle
Yoda1
EGF
+PP2
D
EGFR
SB202190
S1046
S1047
p38
E
Vehicle
Yoda1
EGF
pY1173-EGFR
SB202190
Yoda1+ SB202190
EGF+ SB202190
F
pY1173-EGFR puncta/cell
150
100
50
0
ns
*
**
*
Vehicle
Yoda1
EGF
+SB202190
G
Vehicle
Yoda1
EGF
pS1046/1047
EGFR
1
6.5
2.4
1
3.4
1.5
1
3.2
2.9
Vinculin
+PP2
+SB202190

Fig.3

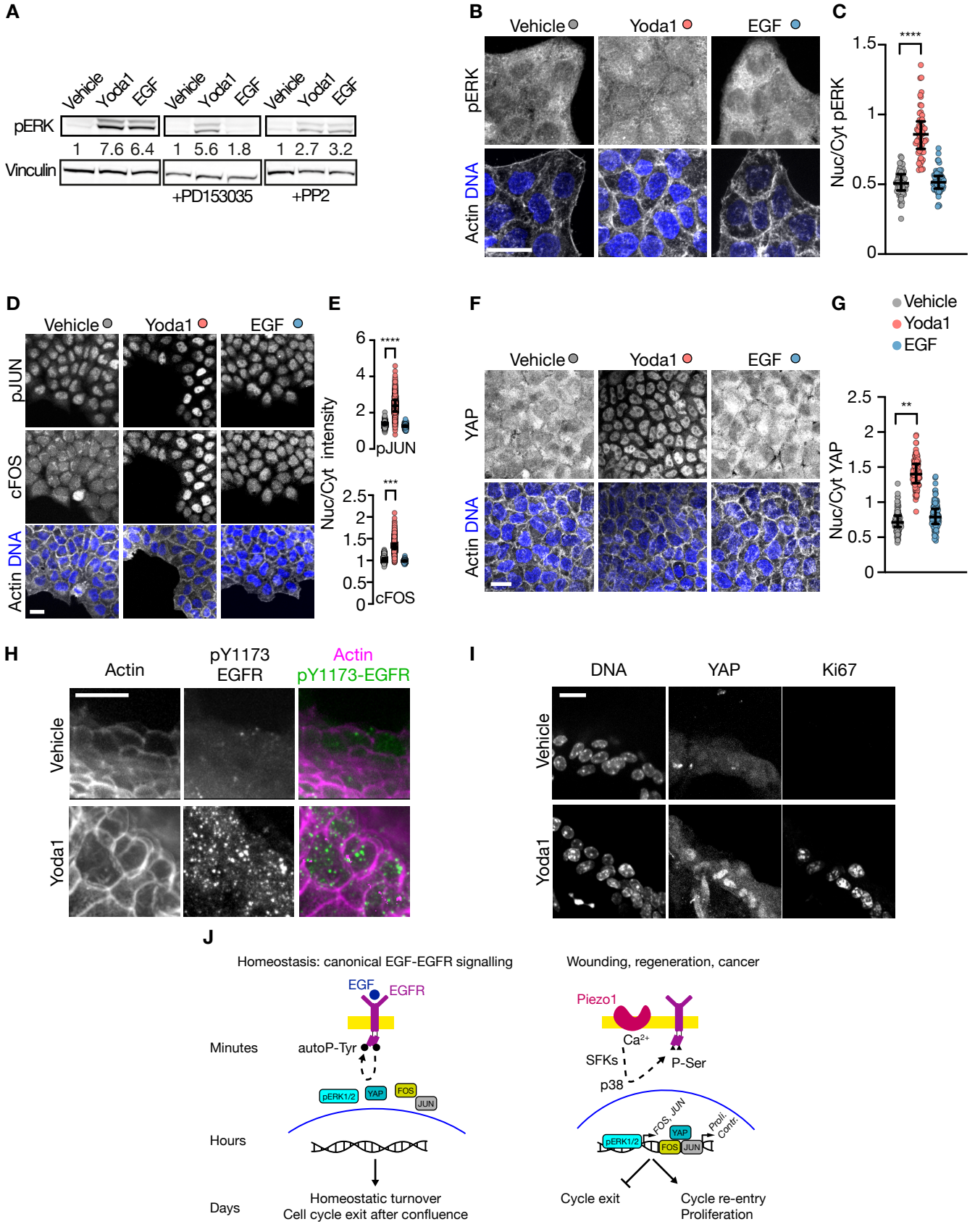
A
Vehicle
Yoda1
EGF
pERK
1 7.6 6.4
1 5.6 1.8
1 2.7 3.2
Vinculin
+PD153035
+PP2
B
Vehicle
Yoda1
EGF
pERK
Actin DNA
C
Nuc/Cyt pERK
****
D
pJUN
cFOS
Actin DNA
E
Nuc/Cyt intensity
pJUN
cFOS
****
***
F
YAP
G
Nuc/Cyt YAP
**
H
Actin
pY1173 EGFR
Actin
pY1173-EGFR
I
DNA
YAP
Ki67
J
Homeostasis: canonical EGF-EGFR signalling
Wounding, regeneration, cancer
EGF
EGFR
Piezo1
Ca2+
Minutes
autoP-Tyr
SFKs
P-Ser
p38
pERK1/2
YAP
FOS
JUN
FOS, JUN
Proli. Contr.
Hours
Days
Homeostatic turnover
Cell cycle exit after confluence
Cycle exit
Cycle re-entry
Proliferation